Environmental Pollution 358 (2024) 124471

Contents lists available at ScienceDirect

Environmental Pollution

journal homepage: www.elsevier.com/locate/envpol

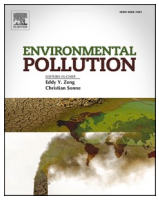

Associations between fine particulate matter, gene expression, and promoter methylation in human bronchial epithelial cells exposed within a classroom under air-liquid interface☆

Massimo Santoro [a,1], Francesca Costabile [b,c,1,*], Maurizio Gualtieri [d], Matteo Rinaldi [c,e], Marco Paglione [c,e], Maurizio Busetto [e], Gianluca Di Iulio [b,f], Luca Di Liberto [b], Monica Gherardi [g], Armando Pelliccioni [g], Paolo Monti [h], Benassi Barbara [a], Maria Giuseppa Grollino [a]

[a] Division of Health Protection Technologies, Italian National Agency for New Technologies, Energy and Sustainable Development (ENEA), 00123, Rome, Italy
[b] Institute of Atmospheric Sciences and Climate - Italian National Research Council (ISAC - CNR), Via Fosso del Cavaliere, 00133, Rome, Italy
[c] NBFC - National Biodiversity Future Center, NBFC, 90133, Palermo, Italy
[d] Department of Earth and Environmental Sciences, University of Milano-Bicocca, Piazza della Scienza 1, 20126, Milan, Italy
[e] Institute of Atmospheric Sciences and Climate - Italian National Research Council (ISAC - CNR), Via Gobetti, 40129, Bologna, Italy
[f] Department of Public Health and Infectious Disease - University of Rome "La Sapienza", via Eudossiana 18, 00184, Rome, Italy
[g] Department of Occupational and Environmental Medicine, Epidemiology and Hygiene, Italian Workers' Compensation Authority (INAIL), Monte Porzio Catone, 00078, Rome, Italy
[h] Department of Civil, Building and Environmental Engineering - University of Rome "La Sapienza", via Eudossiana 18, 00184, Rome, Italy

ARTICLE INFO

Keywords:
Indoor air pollution
Classroom
Ultrafine particles
Black carbon
Polyaromatic hydrocarbons
Particulate matter
Indoor
Epigenetic

ABSTRACT

Associations between indoor air pollution from fine particulate matter (PM with aerodynamic diameter $d_p < 2.5$ μm) and human health are poorly understood. Here, we analyse the concentration-response curves for fine and ultrafine PM, the gene expression, and the methylation patterns in human bronchial epithelial cells (BEAS-2B) exposed at the air-liquid interface (ALI) within a classroom in downtown Rome.

Our results document the upregulation of *aryl hydrocarbon receptor* (*AhR*) and genes associated with xenobiotic metabolism (*CYP1A1* and *CYP1B1*) in response to single exposure of cells to fresh urban aerosols at low fine PM mass concentrations within the classroom. This is evidenced by concentrations of ultrafine particles (UFPs, dp < 0.1 μm), polycyclic aromatic hydrocarbons (PAH), and ratios of black carbon (BC) to organic aerosol (OA). Additionally, an *interleukin 18* (*IL-18*) down-regulation was found during periods of high human occupancy.

Despite the observed gene expression dysregulation, no changes were detected in the methylation levels of the promoter regions of these genes, indicating that the altered gene expression is not linked to changes in DNA methylation and suggesting the involvement of another epigenetic mechanism in the gene regulation.

Gene expression changes at low exposure doses have been previously reported. Here, we add the possibility that lung epithelial cells, when singly exposed to real environmental concentrations of fine PM that translate into ultra-low doses of treatment, may undergo epigenetic alteration in the expression of genes related to xenobiotic metabolism.

Our findings provide a perspective for future indoor air quality regulations. We underscore the potential role of indoor UFPs as carriers of toxic molecules with low-pressure weather conditions, when rainfall and strong winds may favour low levels of fine PM.

☆ This paper has been recommended for acceptance by Admir Créso Targino.

* Corresponding author. Institute of Atmospheric Sciences and Climate - Italian National Research Council (ISAC - CNR), Via Fosso del Cavaliere, 00133, Rome, Italy.
E-mail address: f.costabile@isac.cnr.it (F. Costabile).

[1] These authors contributed equally to the work: Francesca Costabile and Massimo Santoro.

https://doi.org/10.1016/j.envpol.2024.124471
Received 28 February 2024; Received in revised form 25 June 2024; Accepted 27 June 2024
Available online 29 June 2024

1. Introduction

The World Health Organization (WHO) estimates that air pollution is the largest environmental risk to human health (WHO global air quality guidelines, 2021). Several studies have shown that air pollutants, particularly fine particulate matter (aerodynamic diameter $d_p \leq 2.5$ μm; $PM_{2.5}$) and nitrogen dioxide (NO_2), are associated with the onset of various diseases of the respiratory tract, cardiovascular system, cancer, and reduced life expectancy (Chen and Hoek, 2020; Fuller et al., 2022; Huang et al., 2018; Kumar et al., 2023; Yang et al., 2017).

Much of the literature on mortality and morbidity associated with exposure to air pollution focuses on outdoor air pollution, although most exposure occurs indoors (Dimitroulopoulou et al., 2023; Kumar et al., 2023; Morawska et al., 2013).

Although a significant portion of indoor aerosol particles in urban settings are derived from outdoor air, their physicochemical properties undergo profound alterations through outdoor air processing within the ambient indoor air and their mixing with indoor sources, which stem from human and biological emissions and their metabolites, consumer products, and human activities, such as cooking (Goldstein et al., 2021; Kousa et al., 2002; Misztal et al., 2018; Nazaroff, 2023; Wells et al., 2017).

Dynamic processing is important for reactive molecules (Wells et al., 2017), as well as for $PM_{2.5}$, including ultrafine particles (UFPs, $d_p < 0.1$ μm). $PM_{2.5}$ and UFPs are solid or liquid condensed-phase materials in the air and have been studied for their potential adverse health effects, both outdoors and indoors (Costabile et al., 2023; Kwon et al., 2020; Leikauf et al., 2020; Oberdörster et al., 2004).

Complex dynamic processes influence indoor UFPs, including deposition on indoor surfaces, coagulation, nucleation, condensation, evaporation, and sorptive partitioning of semivolatile organic compounds (Nazaroff, 2023). Although negative health effects have been observed indoors, the results are inconsistent, suggesting that indoor processing may produce pollutants with different toxicities (Nazaroff, 2023; Weschler and Wells, 2004; Wolkoff et al., 2006). Although exposure to $PM_{2.5}$ has been associated with adverse health impacts, the understanding of the concentration–response relationships remains incomplete, especially for UFPs at low mass concentrations of $PM_{2.5}$ (Costabile et al., 2023; Stafoggia et al., 2019; Weichenthal et al., 2022).

However, the precise biological mechanisms by which $PM_{2.5}$ affects human health are still being studied and not fully understood (Li et al., 2022). *In vitro* studies have demonstrated deregulation in the expression levels of antioxidant, inflammatory, and unfolded protein response genes in endothelial cells following exposure to air pollutants, such as diesel exhaust particles or $PM_{2.5}$, suggesting a potential mechanism by which air pollution may contribute to cardiopulmonary outcomes (Bengalli et al., 2019; Wang et al., 2019). Another important pathway involved in the response to air pollution is the nuclear factor erythroid 2-related factor 2 (NRF2)-mediated oxidative stress response pathway. The exposure of airway epithelial cells to ambient outdoor $PM_{2.5}$ leads to the upregulation of the *NRF2* gene (Huang et al., 2011).

Moreover, previous studies have shown that prolonged and repeated exposure of bronchial epithelial cells (BEAS-2B) to $PM_{2.5}$ causes inactivation of the NRF2 signalling pathway with impaired mitochondrial redox homeostasis and a subsequent decrease in cellular energy supply (Leclercq et al., 2018). On the other hand, several human studies have demonstrated the potential clinical effects of air pollution from traffic sources. For instance, Peretz et al. (2007) exposed healthy human subjects to diesel exhaust and observed the upregulation of genes related to inflammatory and oxidative stress pathways in peripheral blood mononuclear cells. These findings suggested a link between diesel exhaust exposure, inflammation, and oxidative stress. Another investigation conducted in Los Angeles focused on a cohort of older adults residing in three retirement communities and revealed positive associations between traffic-related pollutants and genes involved in oxidative stress, inflammasome activation, and DNA damage (Wittkopp et al., 2016).

Although human studies as well as *in vivo* and *in vitro* models have provided some insights into the effects of various stimuli on gene expression, it is not yet clear how air pollution affects gene expression in real-world environments with exposure conditions typically found in areas where humans live.

With a novel methodology, Costabile et al. (2023) found that exposure to traffic-related nanoparticles in the urban ambient air at low $PM_{2.5}$ concentrations (<5 μg m^{-3}) may be a source of oxidative stress and inflammation. Pro-inflammatory and oxidative responses, as indicated by *heme oxygenase 1* (*HMOX-1*) and *C-X-C motifchemokine ligand 8* (*CXCL-8*) gene expression, were observed in human bronchial epithelial cells cultured at the air–liquid interface (ALI) and exposed directly to the $PM_{2.5}$/air mixture (no $PM_{2.5}$ filter collection) using a recently developed methodology (Costabile et al., 2017; Gualtieri et al., 2018). This methodology allowed for assessing the low range of $PM_{2.5}$ concentrations (<5 μg m^{-3}) now addressed by the WHO guidelines (WHO global air quality guidelines, 2021).

In this study, we apply this methodology (for the first time, to the best of our knowledge) to an indoor environment within a university classroom in downtown Rome. We exposed BEAS-2B cells to well-characterised indoor aerosols under ALI conditions. The aim was to mimic exposure conditions to real UFP air mixtures representative of human inhalation and deposition and to explore concentration–response relationships within the real range of fine particulate matter concentrations (including the so-called low doses) typically found indoors in a human activity setting (a classroom) in cities in developed countries. We characterised the physicochemical properties of real air mixtures, both indoor and outdoor, using state-of-the-art equipment. These included $PM_{2.5}$, PM_1, UFPs, primary and secondary organic aerosols, black carbon, and polycyclic aromatic hydrocarbons (PAH). A portable ALI exposure module (Cultex RFS compact module) containing the BEAS-2B cell line was used to characterise the biological response to direct exposure to ambient air. We selected 13 genes from different biological pathways involved in responses to air pollution exposure, including oxidative stress, metabolism, and inflammation. Moreover, numerous *in vitro* and *in vivo* studies have shown that PM exposure has a significant impact on DNA methylation patterns (Clifford et al., 2017; Huang et al., 2021; Panni et al., 2016).

DNA methylation is an epigenetic mechanism involving changes in gene expression that do not alter the underlying DNA sequence. The degree of DNA methylation determines whether a gene is actively transcribed or suppressed.

The hypermethylation of promoter regions is generally associated with the suppression of gene expression, whereas hypomethylation is associated with gene activation (Han et al., 2011).

Alterations in DNA methylation can contribute to several diseases, such as cancer (Kulis and Esteller, 2010), autoimmune diseases (Long et al., 2016), and respiratory diseases (Reese et al., 2019).

To understand potential epigenetic responses to indoor air quality and their implications for respiratory health, we analysed DNA methylation changes in BEAS-2B cells after exposure to indoor air pollutants. These findings contribute to a better understanding of the toxicological effects of fine PM concentration–response curves at low doses in real-world indoor environments and their impacts on gene expression and DNA methylation patterns.

2. Material and method

2.1. Description of the measurement site

The measurements were collected in spring 2022 (8–31 March) in the downtown area of Rome (Italy) in the Botany classroom "Giacomini'' of "La Sapienza" University (Fig. 1).

The aerosol measurements were collected both outdoors and indoors. The cells were then exposed solely to indoor conditions. This site

Fig. 1. Location of the measurement sites: 1 indoors, and 2 outdoors.

is representative of the urban background. Major traffic streets are located approximately 500 m from the building. The classroom is on the ground floor, with a theatre arrangement of 20 steps and welcomes 150 students. Owing to COVID-19 restrictions, an average of 60 students occupied the classroom.

The pandemic has influenced indoor conditions. The doors were opened when the students were in a classroom with natural ventilation.

We performed previous measurements in the same classroom, as reported by Pelliccioni et al. (2020).

2.2. Sampling lines

The equipment (described in Sections 2.3–2.5) was placed in a mobile unit outdoors, close to the building, to shorten the sampling lines and minimise particle losses.

We sampled the indoor air at 1.5 m at the end of the theatre steps (i.e. the highest part of the classroom) close to the student seats. The sample lines entered from a small, sealed hole in a large window opposite the entrance door. We sampled the outdoor air near the entrance door.

The sampling lines were copper tubing with a length of 5 m, inner diameter of 4.5 mm, calculated residence time of 1.6 s, and laminar flow conditions. The particle penetration efficiencies into the sampling lines were 96% and 92% for particle diameters (d_p) > 15 nm and >8 nm, respectively, with diffusion losses into the lines being calculated according to literature (Hinds and Zhu, 2022).

The aerosol sampling lines were equipped with a PM_1 head.

The relative humidity of the sampled aerosols was maintained below 30% with Nafion dryers. The cell exposure module sampling line was maintained under ambient conditions. The sampling lines were identical for better comparison of the measurements.

2.3. Equipment for aerosol measurements

The aerosol properties were measured continuously with the same equipment sequentially at fixed intervals, either indoors or outdoors, using a computer-controlled solenoid valve system (Table 1). Initially, the valves were set to switch indoors to outdoors every 7 min. For technical considerations, after 10 d, the valve switch time was adjusted to 10 min.

The fine particle number–size distribution (dry electrical mobility diameter from 8 to 900 nm) was measured using a TROPOS-type mobility particle size spectrometer (MPSS, Wiedensohler et al., 2012) equipped with a butanol-based condensation particle counter (CPC, Model 3772, TSI Inc. USA). The major non-refractory chemical components in PM_1 (sulphate, nitrate, ammonium, chloride, and organics, hereafter indicated as OA) were measured using a high-resolution time-of-flight aerosol mass spectrometer (HR-ToF-AMS, Aerodyne Research Inc., USA), following standard data analysis procedures (Antiñolo et al., 2015; Canagaratna et al., 2007).

A proxy for total PAH in PM1 was derived by summating the potential PAH molecular fragments (C12H8, C12H10, C13H10, C14H10, and C16H10; Antiñolo et al., 2015).

The PAH tracer was validated by comparison with the total PAH measurements performed on the filter samples (Fig. S1).

We used a seven-wavelength (λ = 370, 470, 520, 590, 660, 880, and 950 nm) dual-spot aethalometer (model AE33; Magee Scientific, USA). In the AE33, the mass concentrations of light-absorbing carbonaceous aerosol (LAC) at the different wavelengths are calculated by a built-in algorithm using λ-specific absorption cross-sections provided by the manufacturer. We refer to the LAC aerosol with optical properties and composition like soot particles from fossil fuel combustion as black carbon (BC) (Andreae and Gelencsér, 2006). LAC concentrations at λ = 880 nm are relevant for studies in environments dominated by on-road vehicle exhaust because LAC concentrations at λ < 880 nm have stronger contributions by compounds other than BC (Targino et al., 2024; Weingartner et al., 2003). Therefore, we here provide findings for λ = 880 nm only and refer to the AE33 signal at λ = 880 nm as BC.

The concentrations of regulated air pollutants, such as $PM_{2.5}$, O_3, and NO_2, in the ambient air of Rome were obtained from the ARPA monitoring station located in the nearby Villa Ada (ARPA website; https:

Table 1
Day and time of BEAS-2B exposure. Columns $PM_{0.1}/PM_1$ (#) and $PM_{0.1}/PM_1$ (mass) report the ratio between the number and the mass of the ultrafine particles ($PM_{0.1}$) and PM_1, respectively. In terms of number the UFPs are mostly defining the deposition determined during all the different days of exposure, while in terms of mass, UFPs contribution is always lower than 20%.

Exposure	Start (day-time)	End (day-time)	PM_1 (μg cm^{-2})	PM_1 (cm^{-2})	$PM_{0.1}/PM_1$ (#)	$PM_{0.1}/PM_1$ (mass)
Exp-1	03-08-22, 01:00 p.m.	03-09-22, 01:00 p.m.	$5.97{\cdot}10^{-04}$	$2.41{\cdot}10^{\circ 6}$	96%	16%
Exp-2	03-10-22, 01:00 p.m.	03-11-22, 01:00 p.m.	$1.38{\cdot}10^{-03}$	$3.60{\cdot}10^{\circ 6}$	92%	16%
Exp-3	03-15-22, 01:00 p.m.	03-16-22, 01:00 p.m.	$1.59{\cdot}10^{-03}$	$3.45{\cdot}10^{\circ 6}$	91%	13%
Exp-4	03-17-22, 01:00 p.m.	03-18-22, 01:00 p.m.	$1.54{\cdot}10^{-03}$	$3.41{\cdot}10^{\circ 6}$	92%	12%
Exp-5	03-21-22, 01:00 p.m.	03-22-22, 01:00 p.m.	$1.18{\cdot}10^{-03}$	$3.00{\cdot}10^{\circ 6}$	92%	14%
Exp-6	03-24-22, 01:00 p.m.	03-25-22, 01:00 p.m.	$1.84{\cdot}10^{-03}$	$2.99{\cdot}10^{\circ 6}$	89%	10%
Exp-7	03-28-22, 01:00 p.m.	03-29-22, 01:00 p.m.	$9.95{\cdot}10^{-04}$	$3.32{\cdot}10^{\circ 6}$	94%	15%
Exp-8	03-30-22, 03:00 p.m.	03-31-22, 03:00 p.m.	$9.07{\cdot}10^{-04}$	$2.95{\cdot}10^{\circ 6}$	95%	14%

//www.arpalazio.it/).

2.4. Organic aerosol (OA) source apportionment

OA was apportioned using a positive matrix factorisation (PMF) approach with the Multilinear Engine 2 solver controlled by Source Finder software, SoFi v4.8 (Canonaco et al., 2013; Crippa et al., 2014; Paglione et al., 2020). The standardised source apportionment strategy introduced by Crippa et al. (2014) was performed for the HR-ToF-AMS dataset consisting of organic mass spectra over time and the corresponding errors. Briefly, the PMF aims to derive a linear combination of components that reproduce the observed chemical composition and variations in the time of the measured organic mass spectra (Zhang et al., 2011). The interpretation of the retrieved factors as OA sources was based on an analysis of the mass spectral profiles and their diurnal trends. We apportioned OA into two major primary components without constraints on the solution. Hydrocarbon-like OA (HOA), which represents fresh traffic emissions, was identified based on the prevalence of C3H7+ at m/z 43 and the typical alkene-like structure of the mass spectrum dominated by CxHy ions at m/z 55, 57, 69, and 71. BBOA (biomass burning OA), representing fresh emissions from biomass combustion likely for residential heating, was identified based on m/z 60 and m/z 73 (C2H4O4+ and C3H5O7+). We considered the remaining OA mass (accounting for multiple oxygenated OA and representing secondary OA) as a unique factor (OOA).

2.5. Equipment for meteorological variables

Outdoors, we used the weather station Davis Vantage Pro2, positioned at coordinates 41.889593° N and 12.514564° E. The outdoor meteorological variables considered were wind speed, ws (m s^{-1}), atmospheric pressure (hPa), temperature (°C), and precipitation (mm). These were measured with a 5-min resolution.

The indoor temperature, wind velocity, atmospheric pressure, and relative humidity were measured using two sonic thermometers and anemometers (20 Hz, Gill Instruments Ltd., UK), and differential pressure sensors (1 Hz, Delta Ohm, Italy).

2.6. Cell culture and exposure equipment

The human bronchial epithelial cell line BEAS-2B (RRID: CVCL_0168; ECACC, Salisbury, UK) was maintained as described previously (Gualtieri et al., 2018). Seven days before exposure, 5×10^4 cells were plated on collagen-coated inserts (Corning, NY, USA) grown under submerged conditions to achieve confluence. Twenty-four hours before the exposure, the apical medium was removed and cells were left in the incubator at 37 °C with 5% CO_2.

For cell-based exposure, we used the CULTEX® RFS (Cultex® Technology GmbH, Hannover, Germany), a radial flow system with six different chambers connecting to multi-channel flow controllers (IQ + FLOW, Bronkhorst High-Tech B.V. Ruurlo, Netherlands).

On the day of exposure, the cell-containing inserts were placed into the CULTEX® RFS (Cultex® Technology GmbH, Hannover, Germany) with 4 mL of LHC-9 medium in the basal side of each chamber and transferred to the mobile unit before being connected by a dedicated 5-m-long sampling line.

The sampling line, maintained under laminar ambient conditions, transported indoor air from the classroom to the cell-exposure module.

The ambient air in the classroom was sampled at 1.50 L min^{-1}, with particles with $d_p > 1$ μm being cut by a cyclone. In each chamber of the exposure module, three inserts (numbers 1, 3, and 5) were exposed directly to native air, and three inserts (numbers 2, 4, and 6) were exposed to filtered air and used as internal controls (cells exposed to the same flux, but filtered air). After 24 h of exposure, the cells and media were recovered for subsequent analyses. Eight independent exposures were conducted during the sampling campaign (Table 1).

The theoretical maximum deposited PM_1 number and mass were calculated according to the literature (Aufderheide et al., 2013) with minor modifications. Briefly, aerosol in the atmosphere was used for cell exposure with an airflow rate of 1.50 L min^{-1} for the main inlet and 5 mL min^{-1} for the exposure chamber. Electrical force deposition was not considered in the setup. Size distribution was considered from 8.7 nm to 1 μm to cover the cut-off of the cyclone used.

Particle density was determined according to Hu et al. (2012). The number and mass deposition distributions were calculated and reported considering the cumulative hourly SMPS data (Costabile et al., 2017). The exposure doses were calculated based on the number–size distributions measured using the SMPS. This module was connected to the same sampling line as the cell exposure module.

2.7. Cell viability

The lactate dehydrogenase (LDH) activity was selected as a marker of cell membrane damage and measured in the apical washing and basolateral media collected from control and exposed cells after 24 h of exposure via a CytoTox 96® non-radioactive cytotoxicity assay (Promega, USA) according to the manufacturer's instructions. Samples were read in triplicate using the Glomax Discover System (Promega, USA), which measures absorbance at 490 nm.

2.8. Nucleic acids extraction

Genomic DNA and total RNA were extracted simultaneously from BEAS-2B cells after 24 h of exposure using the AllPrep DNA/RNA Mini Kit (Qiagen, Germany) according to the manufacturer's instructions. The quantity and purity of the extracted nucleic acids were evaluated using a NanoDrop ND-1000 spectrophotometer (Thermo Fisher Scientific, USA).

2.9. Gene expression

First-strand cDNA was synthesised using 1 μg of total RNA using a high-capacity RNA-to-cDNA kit (Thermo Fisher Scientific, USA) according to the manufacturer's instructions.

Quantitative real-time polymerase chain reaction (qRT-PCR) was performed using TaqMan Fast Advanced Master Mix (Thermo Fisher Scientific, USA) and TaqMan probe assays for the following genes involved in different pathways: *Heme Oxygenase 1* (*HMOX1*), *NAD(P)H Quinone Dehydrogenase 1* (*NQO1*), *Superoxide Dismutase 1* (*SOD1*), *Superoxide Dismutase 2* (*SOD2*) [Oxidative Stress], *Aryl Hydrocarbon Receptor* (*AhR*), *Cytochrome P450 Family 1 Subfamily A Member 1* (*CYP1A1*), *Cytochrome P450 Family 1 Subfamily B Member 1* (*CYP1B1*), *NFE2 Like BZIP Transcription Factor 2* (*NFE2L2*) [Metabolism], *NLR Family Pyrin Domain Containing 3* (*NLRP3*), *Interleukin 1 Beta* (*IL-1β*), *Interleukin 6* (*IL-6*), *C-X-C Motif Chemokine Ligand 8* (*IL-8/CXCL8*), *Interleukin 18* (*IL18*) [Inflammation], and *Glyceraldehyde-3-Phosphate Dehydrogenase* (*GAPDH*) as the endogenous control (Table S1).

The thermal cycling conditions on a QuantStudio 5 thermocycler (Thermo Fisher Scientific, USA) consisted of a holding stage at 50 °C for 2 min and 95 °C for 20 s, followed by 40 cycles of each PCR step:

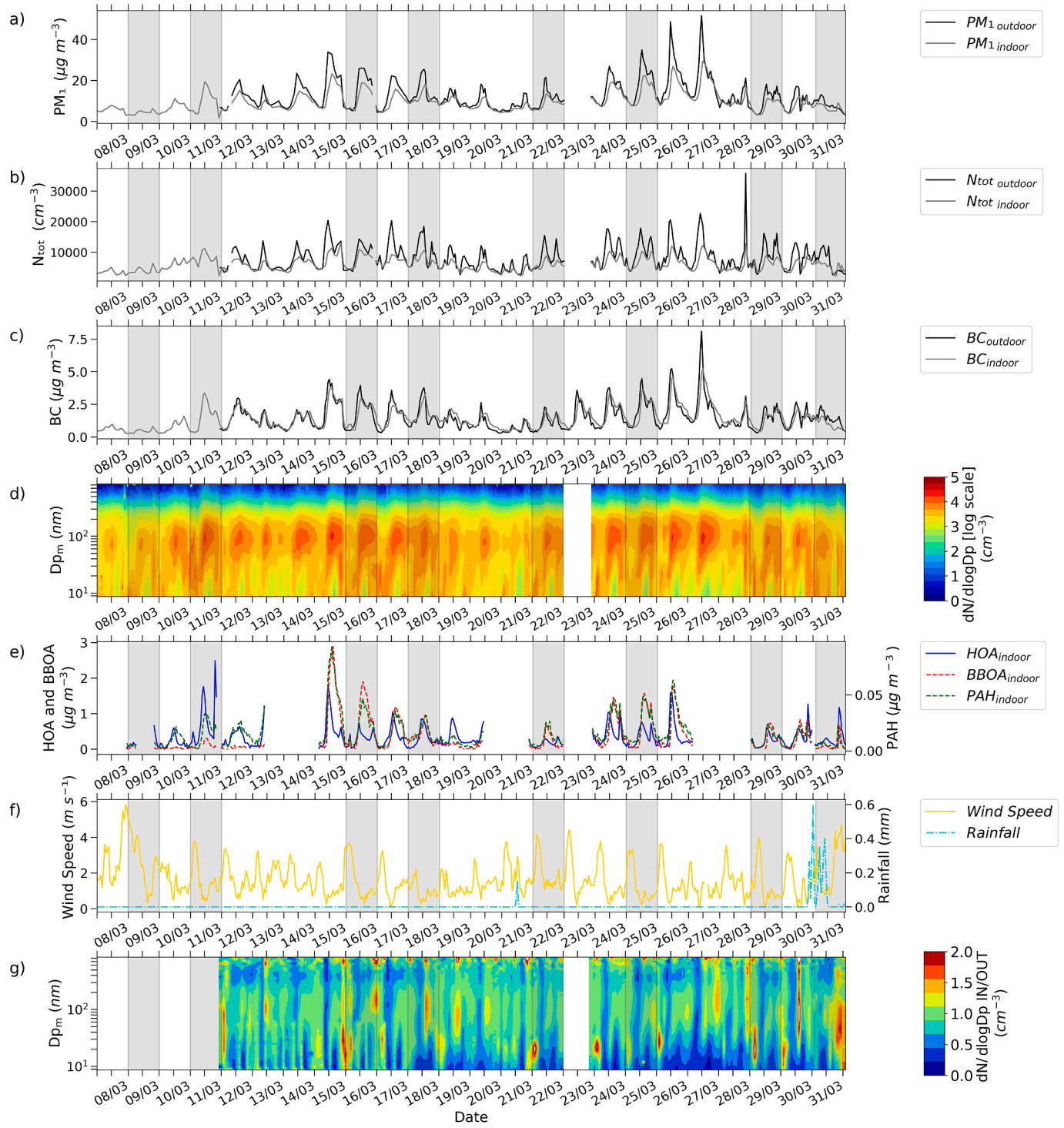

Fig. 2. **a**) Time Series of indoor and outdoor PM_1 mass concentration. **b**) Indoor and outdoor total particle number concentration (N_{tot}). **c**) Black carbon (BC) mass concentration. **D**) Indoor particle number size distribution. **E**) Mass concentration of indoor hydrocarbon-like organic aerosol (HOA), biomass-burning organic aerosol (BBOA), and Polyaromatic Hydrocarbons (PAH). **f**) Wind speed and rainfall, during the whole field. **g**) Indoor-to-outdoor ratios of particle number size distributions (Cell exposure periods are indicated by a grey area).

(denaturation) 95 °C for 1 s and (annealing/extension) 60 °C for 20 s.

We calculated the relative fold change (FC) using the $2^{(-\Delta\Delta CT)}$ method to determine the relative quantitative gene expression. We selected FC > 2 (up-regulation) and FC < 2 (downregulation) with significant changes ($p < 0.05$). The fold change was expressed as a heat map using GraphPad Prism version 8 (GraphPad Software, USA). The p-values were calculated based on a Student's t-test of replicate $2^{(-\Delta CT)}$ values for each gene. All PCRs were performed in triplicate.

2.10. Bisulfite treatment of DNA

Bisulfite treatment of DNA converts all unmethylated cytosines to uracil, leaving the methylated cytosines unaltered. We treated Genomic DNA (1 μg in 20 μL) with EZ DNA Methylation-Gold Kit (Zymo Research, USA) based on the manufacturer's instructions.

2.11. DNA methylation analysis

A DNA methylation study was carried out on genes that showed significant up-regulation (FC > 2 and $p < 0.05$) or downregulation (FC < 2 and $p < 0.05$) during the eight independent exposures (Table 1). For the genes included in the methylation analysis, CpG islands were identified using the online platform MethPrimer (http://www.urogene.org/methprimer/) (Li and Dahiya, 2002).

The complete gene lists, primer sequences, annealing temperatures, and amplicon sizes are provided in Table S2. The specific PCR conditions were 95 °C for 15 min, followed by 50 cycles of 95 °C for 15 s, 60 °C for 30 s, and 70 °C for 30 s, with a final extension of 10 min at 72 °C.

Biotinylated PCR products were processed using a PyroMark Q24 Vacuum Workstation (Qiagen, Germany) and subsequent pyrosequencing was performed on a PyroMark Q24 pyrosequencer using PyroMark Gold Q24 Reagents (Qiagen, Germany).

The methylation percentage at each CpG region was quantified using the PyroMark Q24 software, version 2.0.7 (Qiagen, Germany).

The p-values were calculated based on Student's t-test comparing the methylation percentage of each CpG site in the control vs. the exposed group. The level of significance was set at $p < 0.05$.

3. Results

3.1. Physicochemical aerosol properties

Time series and statistics of the indoor and outdoor aerosol and meteorological variables during the field campaign are shown in Fig. 2, S1, and S2, and Tables 2, 3, S3, and S4.

Fig. 2a–c,e show that the PM_1, OA, and BC mass concentrations indoors followed the outdoor values: the square of the Pearson correlation coefficient (r) among the indoor and outdoor mass concentrations ($r^2_{in\text{-}door\text{-}outdoor}$) was 0.9. The PM_1, OA, and BC mass concentrations tracked the typical urban cycle: lower values at midday and higher at nighttime and during the rush hours. Lower/higher outdoor mass concentrations were observed for higher/lower wind speeds (ws), respectively. This resulted in lower mass concentrations on Exp-1 and Exp-8, and higher mass concentrations on Exp-6, Exp-3, and Exp-4. Fig. 2d shows that the indoor number concentration of particles with $d_p < 0.1$ mm (UFPs) sharply increased during the morning rush hours when the doors were open. In contrast, during the evening rush hours, with closed doors, there was no sharp increase in UFPs. The highest daily values for the indoor total particle number (N_{tot}, Fig. 2b) were measured on Exp-2 and Exp-3, with low values also occurring on Exp-6 and Exp-4. One heavy rain event (Fig. 2f) occurred at the beginning of Exp-8 (as well as light rain on 21 March), and the particle number size distributions (Fig. 2d) after rainfall decreased for UFPs. The primary OAs (HOA and BBOA) and the indoor PAH proxy (Fig. 2e) were higher on Exp-3 and Exp-6.

Fig. 2g shows the indoor-to-outdoor ratios (I/O) for the particle number size distribution (PNSD).

This was assessed based on hourly values to eliminate the time lag between their temporal variations, which varied between 15 and 40 min. The I/O values for the individual aerosol components are presented in Table S3. The HOA (see Section 2.3) was characterised by a median I/O of 1.1 (IQR = 1.1), showing good penetration capability for this traffic-related OA fraction. As for HOA, BC was characterised by a median I/O ratio of 1.0 (IQR = 0.35). The PAH tracer presented an I/O ratio of 0.88 (IQR = 0.46, Table S3).

We observed (Fig. 2g) significant losses of nucleation-mode particles ($N_{8\text{-}30}$) indoors (median I/O = 0.60, IQR = 0.54). This indicates the absence of a major internal source, scarce outdoor penetration capability, and/or quick indoor removal. A higher I/O value (<1) characterised particles in other size ranges.

A minimum occurred for $100 < d_p < 200$ nm (small accumulation-mode particles), probably because of the evaporation of semivolatiles.

Throughout the campaign, the maximum I/O values occurred at $40 < d_p < 100$ nm (soot-mode particles) and $d_p > 200$ nm (large-accumulation-mode particles). The number of indoor nucleation-mode particles ($d_p < 30$ nm, $N_{8\text{-}30}$) was less than half that of the outdoor $N_{8\text{-}30}$.

During Exp-8 and Exp-3, we observed peculiar conditions. On Exp-8, N_{tot} was lower than the average value (owing to low-pressure weather conditions, Fig. 2c), and the I/O ratios for particles with $20 < d_p < 300$ nm were higher (Fig. 2g), especially for soot-mode particles, and lower for particles with $d_p > 400$ nm. On Exp-3, N_{tot} was higher for the Aitken and accumulation-mode particles, and the I/O values were higher for particles with $d_p < 80$ nm.

Wind speed and opening doors affected the aerosol concentrations (Fig. S2). For ws < 1 m s^{-1}, the I/O values were <1, indicating no indoor sources for the particle number and PAH. The I/O values with closed doors were <1, which were lower than those with open doors (approximately 1).

Higher ws occurred in three prevailing directions: (i) NNE, as the site was downwind of a major traffic road; (ii) south, as the site was downwind of a major traffic road; and (iii) west, as the site was downwind of the university campus (Fig. 1).

At higher ws values (1<ws < 3 m s^{-1}), the I/O ratios were larger (larger outdoor aerosol penetration). Under high southerly winds (4<ws < 5 m s^{-1}), the I/O values were >1. This condition occurred on Exp-8, which was also evidenced by the negative value of the pressure delta in Table 2. Indoors, the measurement site was affected by fresh traffic aerosols from nearby streets. We interpret the higher I/O on Exp-8 as follows: (i) the indoor air entered from the door of the classroom (red circle labelled 1, Fig. 1) and arrived from the major southern street; (ii) the outdoor air at the outdoor measurement point (red circle labelled 2, Fig. 1) did not arrive directly from the southern street because of the presence of a tall building located south of the classroom building. The PAH I/O ratios of >1 on Exp-8, even with closed doors (Fig. S2), further demonstrating the good penetration capability of this aerosol at high ws.

3.2. Exposure doses

The exposure data showed differences in the total number or mass dose of PM_1 delivered to the cells (Table 1). The day with the highest deposited mass was Exp-6 ($1.84{\cdot}10^{-3}$ μg cm^{-2}) and the day with the highest number of deposited particles was Exp-2 ($3.6{\cdot}10^{6}$ cm^{-2}). This indicates a clear difference in the information provided by the different exposure metrics. On Exp-1, the lowest deposited doses were observed in terms of mass and number. The different exposure days were ranked according to the deposited mass and number as follows: Exp- 6 > Exp-3 > Exp- 4 > Exp- 2 > Exp-5 > Exp-7 > Exp-8 > Exp-1 and Exp-2 > Exp-4 > Exp-7 > Exp-3 > Exp-5 > Exp-6 > Exp-8 > Exp-1. The relative contribution of the $PM_{0.1}$ (UFPs) number dose was higher on Exp-1 and Exp-2 (96% explained by UFPs); the latter was also the day with the highest mass contribution of UFP (16%).

Table 2
24-h statistics of meteorological variables during the exposure periods outdoors and indoors. Statistics are calculated from 5-min data. The data are indicated as mean, standard deviation and median, interquartile range (IQR), and number of points (#).

Variable		Statistics	Exposure Period							
			EXP-1	EXP-2	EXP-3	EXP-4	EXP-5	EXP-6	EXP-7	EXP-8
Temperature (°C)	Outdoor	Mean	6.3	10.7	12.2	15.3	10.2	13.1	13.9	14.1
		SD	2.9	3.4	3.2	2.5	3.2	4.2	3.2	0.8
		Median	6.0	10.6	12.1	14.9	9.9	12.8	13.8	14.0
		IQR	6.0	5.9	6.1	4.1	6.3	8.0	6.2	1.4
		#	289	289	289	289	288	289	289	289
	Indoor	Mean	18.6	27.1	20.8	21.3	20.3	21.5	22.8	21.9
		SD	4.3	2.3	2.5	1.4	2.4	2.1	2.1	0.8
		Median	16.8	28.0	20.1	20.7	19.5	21.0	22.2	21.6
		IQR	2.6	1.0	3.2	2.6	2.5	1.9	1.8	1.4
		#	287	287	287	244	287	288	283	288
Relative Humidity (%)	Outdoor	Mean	48	57	72	62	47	60	68	88
		SD	11	11	12	6	11	17	11	4
		Median	48	62	79	62	51	66	74	89
		IQR	20	19	22	6	14	31	20	5
		#	289	289	289	289	288	289	289	289
	Indoor	Mean	27	23	41	42	31	33	38	52
		SD	4	3	4	2	4	5	3	2
		Median	28	22	43	43	32	35	39	51
		IQR	6	2	4	2	6	7	3	3
		#	287	287	287	244	287	288	283	288
Pressure (Pa)	Outdoor	Mean	1021	1025	1032	1024	1033	1028	1022	999
		SD	2	1	2	2	1	1	2	3
		Median	1022	1025	1033	1024	1033	1028	1023	997
		IQR	3	1	3	3	2	1	3	6
		#	289	289	289	289	288	289	289	289
Delta Pressure (Pa)	Indoor - Outdoor	Mean	0.01	0.14	−0.61	−0.22	−0.02	0.07	0.15	−1.27
		SD	2.04	1.13	0.85	0.54	1.37	1.07	1.37	0.88
		Median	−0.58	−0.14	−0.56	−0.26	−0.46	−0.26	−0.26	−1.02
		IQR	1.42	0.46	0.50	0.39	1.05	0.70	0.75	1.09
		#	287	287	287	287	287	288	288	288
Wind Speed (m s^{-1})	Outdoor	Mean	2.7	1.6	1.6	1.0	1.9	1.3	1.3	2.5
		SD	1.5	1.1	1.2	0.6	1.0	1.1	1.1	1.5
		Median	2.6	1.4	1.1	0.9	1.6	0.9	0.9	2.3
		IQR	2.4	0.9	1.7	0.7	1.2	1.3	1.2	2.6
		#	289	289	289	289	287	289	289	289

3.3. Expression analysis

To correlate gene expression data with indoor air pollution, we performed ALI exposure of BEAS-2B from 8 March to 30 March (2022) at the same location as the aerosol measurements.

During the eight exposures, cell viability showed no significant differences among the exposed (chambers 1, 3, and 5) and control cells (chambers 2, 4, and 6), as determined by LDH release in the apical and basolateral media as a marker for cell membrane damage (Fig. S3). The expression levels of 13 genes involved in oxidative stress, metabolism, and inflammation (Table S1) were evaluated in exposed and control cells. The analysis was based on significant changes ($p < 0.05$) that were at least 2-fold up- or downregulated compared with the controls. Using these criteria, we found that, on Exp-3 (Table 1), the *IL-18* gene was significantly downregulated (fold change = 0.36, $p = 0.049$) in the exposed cells compared with the control (Fig. 3).

Moreover, in Exp-8 (Table 1), by comparing the exposed and control cells, we observed a significant up-regulation of the following three genes: *AhR* with a fold change of 2.37 ($p = 0.047$), *CYP1A1* with a fold change of 3.67 ($p = 0.028$), and *CYP1B1* with a fold change of 3.78 ($p = 0.038$) (Fig. 3).

3.4. DNA methylation analysis

DNA methylation analysis focused on four genes that showed significant dysregulation in the exposed cells compared with the control cells: *IL-18* (Exp-3), *AhR*, *CYP1A1,* and *CYP1B1* (Exp-8).

Using pyrosequencing analysis, we found different methylation levels of five CpG sites analysed in the promoter region of the *IL-18* gene: CpG1 showed an average methylation level of 18–20%, CpG2, CpG4, and CpG5 displayed an average methylation level of 40–60%, and CpG3 showed a methylation level of 85–90% without differences between exposed and control cells (Fig. 4a).

The promoter region of the *AhR* gene displayed an average methylation level of 3–7% in both control and exposed cells for the eight CpG sites analysed (Fig. 4b).

For *CYP1A1*, we analysed 13 CpG sites in the promoter region and found average methylation levels of 4–6% for CpG2, CpG3, CpG4, CpG6, CpG7, CpG10, CpG11, and CpG13. CpG1, CpG5, CpG8, CpG9, and CpG12 showed average methylation levels of 10–20% in both control and exposed cells (Fig. 4c). Finally, six CpG sites within the *CYP1B1* promoter region displayed hypomethylation (2–8%), with no significant differences between control and exposed cells (Fig. 4d).

3.5. Concentration–response curves for $PM_{0.1}$ and gene expression patterns

Fig. 5 shows the concentration–response curves for $PM_{0.1}$ and the gene expression patterns. The figure displays (as the colour of the data points) the condensation sink (CS) of the accumulation-mode particles ($d_p > 100$ nm, $CS > 10_0$) and the BC-to-OA ratio (size of the data point). Fig. S4 shows the same plot, except with PM_1 on the x-axis, indicating the mass concentration of $PM_{2.5}$. $CS_{>100}$ is directly correlated with the PM_1 mass concentration; accumulation-mode particles mostly contributed to mass.

A low $CS > 100$ value is an indication of atmospheric conditions when condensable compounds (including ROS) do not sink rapidly onto pre-existing accumulation-mode particles and may be scavenged by or form nanoparticles (Costabile et al., 2023).

A high BC-to-OA ratio indicates fresh combustion aerosols (Saleh

Table 3
Descriptive statistics of aerosol parameters measured indoors and outdoors during the exposure periods (time resolution of data 7–10 min). PM_1: mass concentration of particulate matter with aerodynamic diameter <1 μm; N_{tot}: total particle number concentration; BC: Black Carbon mass concentration; OA: organic aerosol mass concentration; HOA: hydrocarbon-like organic aerosol mass concentration; BBOA: biomass burning organic aerosol mass concentration; PAH: polyaromatic hydrocarbon mass concentration.

Aerosol Measurements		Statistic	Exposure							
			EXP-1	EXP-2	EXP-3	EXP-4	EXP-5	EXP-6	EXP-7	EXP-8
PM_1 ($\mu g\ m^{-3}$)	Indoor	Mean	4	10	12	11	9	14	8	7
		SD	1	6	6	3	2	5	3	2
		Median	4	11	13	10	9	13	9	6
		IQR	1	8	11	3	4	10	6	3
		#	44	40	36	72	71	72	72	72
	Outdoor	Mean			16	14	11	18	10	8
		SD			9	6	4	8	5	3
		Median			19	12	10	18	10	7
		IQR			18	4	5	15	9	4
		#			37	73	72	73	73	72
N_{tot} (cm^{-3})	Indoor	Mean	3908	7736	7514	7159	6069	6972	6281	5175
		SD	1088	2581	2572	1676	1220	2079	1714	1567
		Median	3506	8109	8635	6925	5949	7003	6544	5594
		IQR	1477	2409	4781	2719	1647	3509	2743	2333
		#	44	40	36	72	71	72	72	72
	Outdoor	Mean			8881	9600	8299	9567	8782	6478
		SD			4124	4607	3253	4179	4051	3692
		Median			9129	8727	7833	9417	8226	5637
		IQR			8250	5911	4262	7035	4579	5689
		#			37	73	72	73	73	72
BC ($ng\ m^{-3}$)	Indoor	Mean	449.3	1593.0	1770.9	1758.4	1164.4	1963.7	1338.6	964.5
		SD	158.3	1025.0	961.5	739.2	520.0	1092.1	696.1	463.5
		Median	433.0	1736.0	2083.0	1535.5	1196.0	1888.0	1498.0	904.5
		IQR	213.0	1746.5	1676.5	971.3	848.0	1876.8	1235.0	670.5
		#	503	475	503	574	501	558	560	534
	Outdoor	Mean			1907.7	1682.8	1100.1	2052.2	1377.7	1365.0
		SD			1175.2	1009.9	639.7	1209.0	819.9	759.7
		Median			2098.0	1350.5	1015.5	1920.0	1392.5	1211.0
		IQR			1983.3	971.0	927.8	1815.8	1366.3	895.5
		#			480	558	512	560	558	574
OA ($\mu g\ m^{-3}$)	Indoor	Mean	2.31	4.04	5.77	5.87	4.70	7.19	3.46	2.34
		SD	0.48	2.17	1.78	1.37	0.90	1.87	0.93	0.93
		Median	2.21	3.86	6.11	6.04	4.48	6.57	3.67	2.20
		IQR	0.46	4.09	3.08	1.81	1.17	3.55	1.59	0.88
		#	84	177	103	72	71	71	71	72
	Outdoor	Mean			7.61	6.86	5.71	9.29	4.39	2.30
		SD			4.18	2.73	2.11	3.78	1.93	0.78
		Median			8.09	6.01	5.11	9.57	4.78	2.12
		IQR			6.82	3.29	1.86	6.11	3.29	1.10
		#			103	72	73	72	71	72
HOA ($\mu g\ m^{-3}$)	Indoor	Mean	0.26	0.74	0.52	0.54	0.30	0.56	0.41	0.48
		SD	0.23	0.76	0.33	0.42	0.15	0.41	0.29	0.46
		Median	0.17	0.45	0.53	0.36	0.30	0.46	0.41	0.34
		IQR	0.18	0.83	0.40	0.51	0.22	0.71	0.42	0.24
		#	79	177	95	67	71	70	71	72
BBOA ($\mu g\ m^{-3}$)	Indoor	Mean	0.04	0.14	1.20	0.66	0.37	1.05	0.50	0.20
		SD	0.04	0.14	1.07	0.41	0.39	0.91	0.42	0.32
		Median	0.03	0.08	0.96	0.56	0.17	0.67	0.38	0.09
		IQR	0.04	0.20	2.02	0.40	0.56	1.58	0.76	0.15
		#	29	114	99	70	63	67	56	57
PAH ($\mu g\ m^{-3}$)	Indoor	Mean	0.01	0.02	0.02	0.02	0.01	0.02	0.01	0.01
		SD	0.00	0.01	0.02	0.01	0.01	0.02	0.01	0.01
		Median	0.00	0.01	0.02	0.01	0.01	0.02	0.01	0.00
		IQR	0.00	0.02	0.02	0.01	0.01	0.02	0.01	0.00
		#	82	177	103	72	71	71	71	72

et al., 2014), with lower values for aged aerosols.

Fig. 5 and S4 show that the data points of aged aerosols (low BC-to-OA ratio) were on the right side of the plot (higher $PM_{0.1}$, PM_1, and $PM_{2.5}$ mass concentrations) and associated with larger $CS_{>100}$. Among these data points with higher mass concentrations, we did not observe any statistically significant gene expression, except for Exp-3, where we observed downregulation of the *IL-18* gene. Data points with lower $CS_{>100}$ and higher BC-to-OA ratios were on the left side of the plots and identified exposure to fresh combustion aerosols. Among these, on Exp-8 we observed high expression patterns of several genes, including *AhR*, *CYP1A1,* and *CYP1B1*.

Exp-8 was the only day with low-pressure weather conditions and rainfall (Fig. 2, Table 2) at the beginning of the 24-h exposure period. Rainfall decreased the PM_1 mass concentration and $CS_{>100}$. Strong southerly winds persisted during rush hour at the end of the exposure period (Fig. 2). Fig. 2g shows that, at the end of Exp-8, with open doors, strong southerly winds caused a large penetration of fresh urban aerosol particles (particularly from a southern traffic road) indoors during rush hours. This was indicated by the high I/O ratios for UFPs and the PAH peak (Fig. S2).

We also observed a concurrent low $CS > 100$, due to the outdoor rain scavenging.

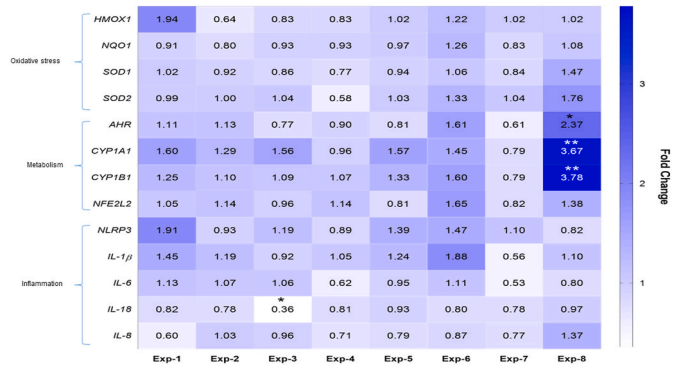

Fig. 3. Heat map representation of fold changes. Upregulation and down-regulation of gene expression levels are indicated in blue and white boxes respectively. Student's t-test of control vs. exposed cells * ($p < 0.05$) and ** ($p < 0.02$). (For interpretation of the references to colour in this figure legend, the reader is referred to the Web version of this article.)

Fig. 5 and S4 show no statistically significant correlation between the $PM_{0.1}$ and fine PM mass concentrations, and the biological responses.

4. Discussion

In this study, we exposed BEAS-2B cells under ALI conditions indoors to urban aerosols within a university classroom in downtown Rome (Fig. 1) in the spring of 2022. We characterised fine aerosol physicochemical properties using state-of-the-art equipment and assessed biological responses through the expression and methylation profiles of 13 genes involved in various biological pathways (Table S1). The aim was to explore the concentration–response relationships for fine PM in an urban background indoor environment.

During Exp-8 (Table 1), we observed significant upregulation of *AhR, CYP1A1,* and *CYP1B1* genes (Fig. 3). We identified a statistically significant association between the deregulation of these genes and fresh combustion-generated aerosols at low PM_1 levels (Fig. 5). Exp-8 was characterised by the indoor penetration of traffic-related nanoparticles (down to 8 nm, Fig. 2g) with higher PAH content and BC-to-OA ratios and low PM_1 concentrations (Figs. 2 and 5) during traffic rush hours.

The observed biological response to this fresh indoor urban aerosol is consistent with our recent findings (Costabile et al., 2023). Consistent with the present observations, the previous biological response occurred on winter weekdays, when traffic rush hours followed low-pressure weather conditions. Rainfall and strong winds caused (both outdoor and indoor) decreases in accumulation-mode particles and thus PM_1 mass concentration, resulting in a low condensation sink of particles with a $d_p > 0.1$ μm (or 100 nm, $CS_{>100}$, Fig. 5 and S4). At low $CS_{>100}$, toxic molecules (such as the PAH observed in Fig. 2) could be enriched in nanoparticles rather than in accumulation-mode particles.

This may elicit a more potent toxicological response in agreement with a Trojan-horse mechanism for nanoparticles acting as carriers for toxics (Costabile et al., 2023; Gualtieri et al., 2018).

Notably, on Exp-8 we observed low deposition doses in terms of particle mass and number. These results indicate that the "classical" metrics used for human health protection are not predictive of possible

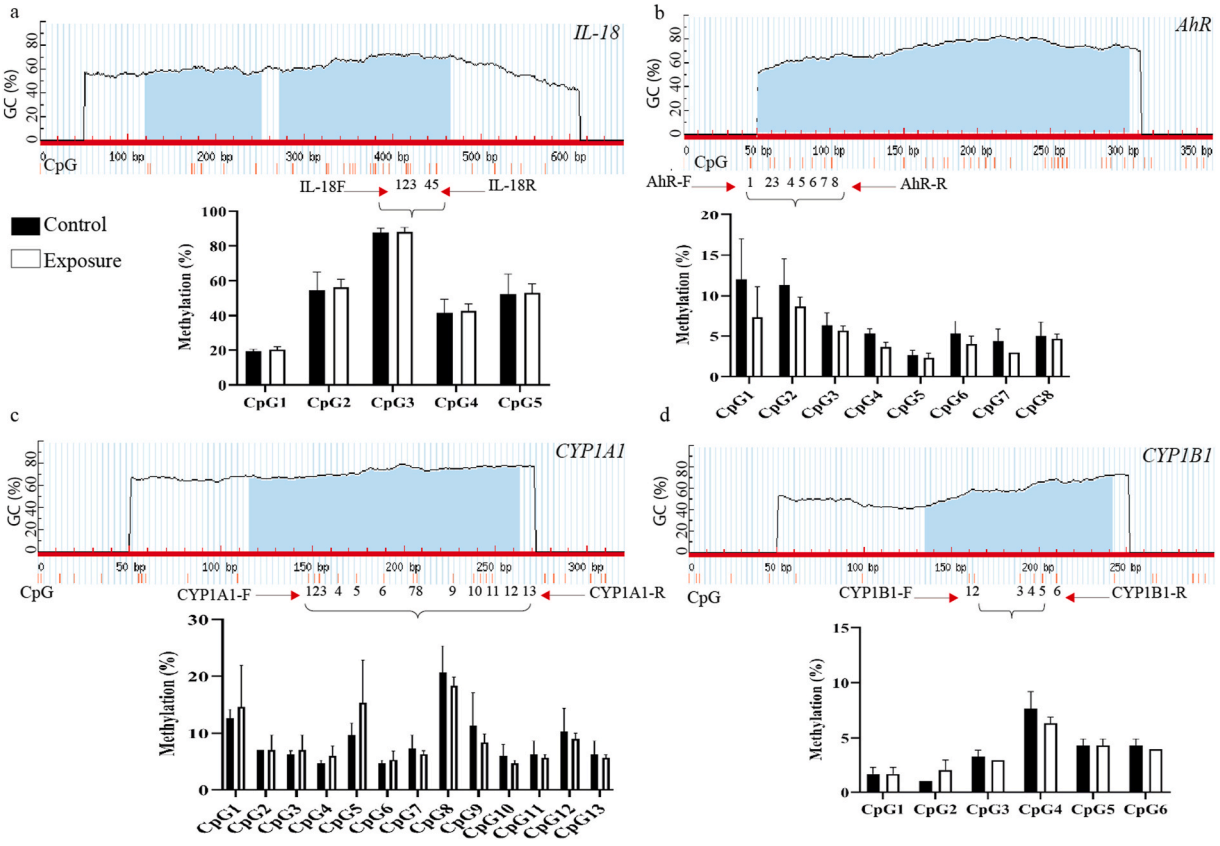

Fig. 4. Methylation analysis of *IL-18, AhR, CYP1A1* and *CYP1B1* loci by pyrosequencing. Up panels showed CpG islands (blue region) identified by the MethPrimer program (Li and Dahiya, 2002). a) *IL-18* promoter region with vertical red bars that indicated the position of CpG sites numbered from 1 to 5. The PCR primers used in this study are indicated as arrows. Lower panel: Histogram of the average methylation percentage in control (black) and exposed cells (white). b, c and d) *AhR, CYP1A1* and *CYP1B1* promoter regions respectively. Vertical red bars indicated the position of CpG sites numbered from 1 to 8 for *AhR*, from 1 to 13 for *CYP1A1* and from 1 to 6 for *CYP1B1*. The PCR primers used in this study are indicated as arrows. Lower panel: Histogram of the average methylation percentage in control (black) and exposed cells (white). (For interpretation of the references to colour in this figure legend, the reader is referred to the Web version of this article.)

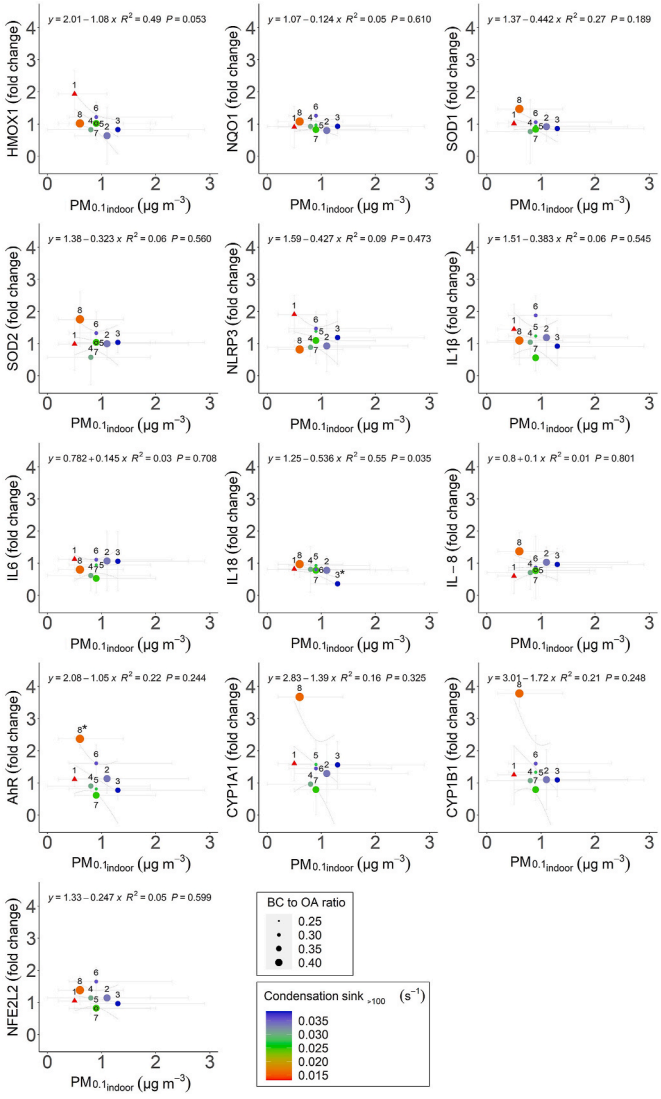

Fig. 5. Concentration-response curves for $PM_{0.1}$ and gene expression patterns. Datapoints are colored by the condensation sink calculated for particles larger than 100 nm and sized by the black carbon to organic aerosol (BC-to-OA) ratio. Statistics: medians and St.dev. Linear regression curves with Confidence Intervals are shown.

epigenetic alterations.

Gene expression changes at low exposure doses have been previously reported. Here, we demonstrated that lung epithelial cells, when singly exposed to real environmental concentrations of fine PM that translate into ultra-low doses of treatment, may undergo epigenetic alterations in the expression of genes related to xenobiotic metabolism.

AhR is a cytosolic receptor that is activated by binding to certain environmental chemicals, such as PAH and persistent organic pollutants (POPs) (Vogel et al., 2019; Weng et al., 2018). After AhR binds to its ligands and translocates to the nucleus, it binds to specific DNA regulatory sequences, such as xenobiotic-responsive elements (XREs) (also known as dioxin-responsive elements) (Vogel et al., 2019). This determines the expression of phase I enzymes, such as *CYP1A1*, *CYP1A2*, and *CYP1B1*, and phase II enzymes, such as *NQO1, Glutathione S-Transferase Alpha 2* (*GST-A2*), *UDP Glucuronosyltransferase Family 1 Member A1* (*UGT1A1*), and *UDP Glucuronosyltransferase Family 1 Member A6* (*UGT1-A6*) (Nebert, 2017; Rothhammer and Quintana, 2019; Vogel et al., 2019). The upregulation of *CYP1A1* and *CYP1B1* is consistent with *AhR*'s role in the activation of phase I xenobiotic-metabolising enzymes, which are essential for metabolising and activating xenobiotics. In addition, the upregulation of *AhR*, *CYP1A1*, and *CYP1B1* was not due to changes in DNA methylation of their promoter regions (Fig. 2b–d). This agrees with Miura et al. (2021), who found, in βNF-exposed HepG2 cells, a preferential binding of activated AhR to unmethylated XRE sequences located in the transcriptional regulatory regions of *CYP1A1* and *CYP1B1*. It is likely that the regulation of these genes involves additional epigenetic mechanisms, including histone acetylation, hydroxymethylation, microRNAs, and long non-coding RNA, as well as exposure to environmental chemicals.

In contrast, we observed significant downregulation of the *IL-18* gene on Exp-3 (Fig. 3). IL-18 is a product of inflammasome activation and plays a critical role in the inflammatory response by promoting the activation of immune cells and other proinflammatory molecules (Pinkerton et al., 2017). This cytokine is activated in response to various stimuli, including pathogens (such as bacteria and viruses), environmental factors, and host-derived danger signals. No changes in DNA methylation were observed in the *IL-18* promoter region (Fig. 4a).

Fig. 2g shows an increase in the I/O ratios for nucleation-mode particles at the beginning of Exp-3 (at approximately 14:00), but this was not associated with any increase in organic compounds, as was the case on Exp-8 (i.e. during rush hour, Fig. 2). In addition, at the end of Exp-3 (at approximately 12:00), an increase in the I/O for accumulation-mode particles occurred. However, the PAH concentration was high but not higher than that during other exposure periods (e.g., Exp-6). Interestingly, Exp-3 was associated with the highest number of students in classrooms during the COVID-19 period. We speculate that the observed inflammatory response may be related to the exposure to pathogens because of the relatively high number of individuals in the classroom. On the other hand, Exp-3 was characterised by the highest BBOA concentration among the exposure days; a possible role of biomass burning should also be considered, as already reported in the literature (Pardo et al., 2020; Park et al., 2018).

Finally, we used BEAS-2B cells derived from normal bronchial epithelium. These cells have inherent limitations, such as low differentiation levels, low levels of tight junctions, and the absence of MUC5AC expression, which plays a critical role in mucociliary clearance (Stewart, 2012). Despite these limitations, BEAS-2B cells are reliable for investigating various biological aspects, such as cell structure, metabolism, inflammation, and oxidative stress (Kinnula et al., 2012; McGovern et al., 2010). Notably, several studies have employed BEAS-2B cells under ALI conditions to simulate aerosol exposure *in vitro*, using Cultex RFS or Vitrocell® exposure systems (Costabile et al., 2023; Gualtieri et al., 2018; McGovern et al., 2010; Weber et al., 2013). However, further studies are required to validate these findings. In particular, the characterisation of other cell lines derived from different bronchial regions, such as mucus- or surfactant-producing cells, macrophages, and other immune cells, may help in exploring the possible combined effects of different cell types that were not considered in this study.

5. Conclusions

We characterised the gene expression and DNA methylation patterns, together with the physicochemical properties of fine and ultrafine aerosols within a university classroom, in downtown Rome using a novel methodology. The findings demonstrate the influence of outdoor aerosol sources (primarily urban vehicular traffic) on indoor aerosol toxicity. The findings also demonstrated how this influence was modulated in a complex manner by weather conditions and indoor air processing. This typically occurs in urban areas during traffic rush hours and low-pressure weather events in winter. During traffic rush hour, fresh vehicle emissions occur after rainfall and strong winds may decrease the mass concentration of accumulation-mode particles (and thus their CS). These conditions may favour an increase in traffic-related nanoparticles associated with PAH at low indoor levels of fine PM. Under these conditions, we observed the upregulation of *AhR* and genes related to xenobiotic metabolism (*CYP1A1* and *CYP1B1*). Moreover, we observed

downregulation of *IL-18* during high student occupancy (possibly associated with biomass-burning aerosols), with no changes in their DNA methylation levels.

Our findings provide a perspective for future indoor air quality regulations, with recommendations for indoor air quality metrics. These metrics should consider how potentially toxic molecules in the air mixture are distributed between fine and ultrafine particles.

Funding

This research was funded by the Italian Workers' Compensation Authority (INAIL) in the frame of its scientific research programs (2019–2021).

CNR-ISAC acknowledges financial support from PNRR MUR project ECS_00000033_ECOSISTER.

CRediT authorship contribution statement

Massimo Santoro: Writing – review & editing, Writing – original draft, Methodology, Investigation, Formal analysis, Data curation, Conceptualization. **Francesca Costabile:** Writing – review & editing, Writing – original draft, Project administration, Methodology, Investigation, Funding acquisition, Formal analysis, Data curation, Conceptualization. **Maurizio Gualtieri:** Writing – review & editing, Conceptualization. **Matteo Rinaldi:** Writing – review & editing, Methodology, Data curation, Conceptualization. **Marco Paglione:** Writing – review & editing, Methodology, Data curation. **Maurizio Busetto:** Methodology. **Gianluca Di Iulio:** Data curation. **Luca Di Liberto:** Methodology. **Monica Gherardi:** Funding acquisition, Data curation. **Armando Pelliccioni:** Funding acquisition, Data curation. **Paolo Monti:** Funding acquisition. **Benassi Barbara:** Writing – review & editing. **Maria Giuseppa Grollino:** Writing – review & editing, Project administration, Methodology, Funding acquisition, Data curation.

Declaration of competing interest

The authors declare that they have no known competing financial interests or personal relationships that could have appeared to influence the work reported in this paper.

Data availability

Data will be made available on request.

Acknowledgments

The authors are grateful to the entire research team of the BRIC project. We acknowledge the precious support from ARPA Lazio, to obtain data of regulated air pollutants at the close urban background monitoring station located in the nearby Villa Ada (ARPA website; https://www.arpalazio.it/). We also acknowledge the support of the ASTI network providing meteorological data.

Appendix A. Supplementary data

Supplementary data to this article can be found online at https://doi.org/10.1016/j.envpol.2024.124471.

References

Andreae, M.O., Gelencsér, A., 2006. Black carbon or brown carbon? The nature of light-absorbing carbonaceous aerosols. Atmos. Chem. Phys. 6 (10), 3131–3148.

Antiñolo, M., Willis, M.D., Zhou, S., Abbatt, J.P.D., 2015. Connecting the oxidation of soot to its redox cycling abilities. Nat. Commun. 6 https://doi.org/10.1038/NCOMMS7812.

Aufderheide, M., Halter, B., Möhle, N., Hochrainer, D., 2013. The CULTEX RFS: a comprehensive technical approach for the in vitro exposure of airway epithelial cells to the particulate matter at the air-liquid interface. BioMed Res. Int. 2013 https://doi.org/10.1155/2013/734137.

Bengalli, R., Zerboni, A., Marchetti, S., Longhin, E., Priola, M., Camatini, M., et al., 2019. In vitro pulmonary and vascular effects induced by different diesel exhaust particles. Toxicol. Lett. 306, 13–24. https://doi.org/10.1016/J.TOXLET.2019.01.017.

Canagaratna, M.R., Jayne, J.T., Jimenez, J.L., Allan, J.D., Alfarra, M.R., Zhang, Q., et al., 2007. Chemical and microphysical characterization of ambient aerosols with the aerodyne aerosol mass spectrometer. Mass Spectrom. Rev. 26, 185–222. https://doi.org/10.1002/MAS.20115.

Canonaco, F., Crippa, M., Slowik, J.G., Baltensperger, U., Prévôt, A.S.H., 2013. SoFi, an IGOR-based interface for the efficient use of the generalized multilinear engine (ME-2) for the source apportionment: ME-2 application to aerosol mass spectrometer data. Atmos. Meas. Tech. 6, 3649–3661. https://doi.org/10.5194/AMT-6-3649-2013.

Chen, J., Hoek, G., 2020. Long-term exposure to PM and all-cause and cause-specific mortality: a systematic review and meta-analysis. Environ. Int. 143 https://doi.org/10.1016/J.ENVINT.2020.105974.

Clifford, R.L., Jones, M.J., MacIsaac, J.L., McEwen, L.M., Goodman, S.J., Mostafavi, S., et al., 2017. Inhalation of diesel exhaust and allergen alters human bronchial epithelium DNA methylation. J. Allergy Clin. Immunol. 139, 112–121. https://doi.org/10.1016/J.JACI.2016.03.046.

Costabile, F., Alas, H., Aufderheide, M., Avino, P., Amato, F., Argentini, S., et al., 2017. First results of the "carbonaceous aerosol in Rome and environs (CARE)" experiment: beyond current standards for PM10. Atmos 8. https://doi.org/10.3390/ATMOS8120249. Page 249 2017;8:249.

Costabile, F., Gualtieri, M., Rinaldi, M., Canepari, S., Vecchi, R., Massimi, L., et al., 2023. Exposure to urban nanoparticles at low PM_1concentrations as a source of oxidative stress and inflammation. Sci. Rep. 13 https://doi.org/10.1038/S41598-023-45230-Z.

Crippa, M., Canonaco, F., Lanz, V.A., Äijälä, M., Allan, J.D., Carbone, S., et al., 2014. Organic aerosol components derived from 25 AMS data sets across Europe using a consistent ME-2 based source apportionment approach. Atmos. Chem. Phys. 14, 6159–6176. https://doi.org/10.5194/acp-14-6159-2014.

Dimitroulopoulou, S., Dudzi'nskadudzi'nska, M.R., Gunnarsen, L., Hägerhed, L., Maula, H., Singh, R., et al., 2023. Indoor air quality guidelines from across the world: an appraisal considering energy saving, health, productivity, and comfort. Environ. Int. 178, 108127 https://doi.org/10.1016/j.envint.2023.108127.

Fuller, R., Landrigan, P.J., Balakrishnan, K., Bathan, G., Bose-O'Reilly, S., Brauer, M., et al., 2022. Pollution and health: a progress update. Lancet Planet Heal 6, e535–e547. https://doi.org/10.1016/S2542-5196(22)00090-0.

Goldstein, A.H., Nazaroff, W.W., Weschler, C.J., Williams, J., 2021. How do indoor environments affect air pollution exposure? Environ. Sci. Technol. 55, 100–108. https://doi.org/10.1021/ACS.EST.0C05727.

Gualtieri, M., Grollino, M.G., Consales, C., Costabile, F., Manigrasso, M., Avino, P., et al., 2018. Is it the time to study air pollution effects under environmental conditions? A case study to support the shift of in vitro toxicology from the bench to the field. Chemosphere 207, 552–564. https://doi.org/10.1016/J.CHEMOSPHERE.2018.05.130.

Han, H., Cortez, C.C., Yang, X., Nichols, P.W., Jones, P.A., Liang, G., 2011. DNA methylation directly silences genes with non-CpG island promoters and establishes a nucleosome occupied promoter. https://doi.org/10.1093/hmg/ddr356.

Hinds, W.C., Zhu, Y., 2022. Aerosol Technology: Properties, Behavior, and Measurement of Airborne Particles, third ed. Wiley, p. 448.

Hu, M., Peng, J., Sun, K., Yue, D., Guo, S., Wiedensohler, A., et al., 2012. Estimation of size-resolved ambient particle density based on the measurement of aerosol number, mass, and chemical size distributions in the winter in Beijing. Environ. Sci. Technol. 46, 9941–9947. https://doi.org/10.1021/ES204073T.

Huang, J., Pan, X., Guo, X., Li, G., 2018. Impacts of air pollution wave on years of life lost: a crucial way to communicate the health risks of air pollution to the public. Environ. Int. 113, 42–49. https://doi.org/10.1016/J.ENVINT.2018.01.022.

Huang, S.K., Tripathi, P., Koneva, L.A., Cavalcante, R.G., Craig, N., Scruggs, A.M., et al., 2021. Effect of concentration and duration of particulate matter exposure on the transcriptome and DNA methylome of bronchial epithelial cells. Environ Epigenetics 7. https://doi.org/10.1093/EEP/DVAA022.

Huang, Y.C.T., Karoly, E.D., Dailey, L.A., Schmitt, M.T., Silbajoris, R., Graff, D.W., et al., 2011. Comparison of gene expression profiles induced by coarse, fine, and ultrafine particulate matter. J. Toxicol. Environ. Health 74, 296–312. https://doi.org/10.1080/15287394.2010.516238.

Kinnula, V.L., Yankaskas, J.R., Chang, L., Virtanen, I., Linnala, A., Kang, B.H., et al., 2012. Primary and immortalized (BEAS 2B) human bronchial epithelial cells have significant antioxidative capacity in vitro 11, 568–576. https://doi.org/10.1165/AJRCMB.11.5.7946385. Https://DoiOrg/101165/Ajrcmb1157946385.

Kousa, A., Kukkonen, J., Karppinen, A., Aivi Aarnio, P., Koskentalo, T., 2002. A model for evaluating the population exposure to ambient air pollution in an urban area. Atmos. Environ. 36, 2109–2119.

Kulis, M., Esteller, M., 2010. Chapter 2 - DNA methylation and cancer. Epigenetics Cancer, Part A 70, 27–56.

Kumar, P., Singh, A.B., Arora, T., Singh, S., Singh, R., 2023. Critical review on emerging health effects associated with the indoor air quality and its sustainable management. https://doi.org/10.1016/j.scitotenv.2023.162163.

Kwon, H.S., Ryu, M.H., Carlsten, C., 2020. Ultrafine particles: unique physicochemical properties relevant to health and disease. Exp. Mol. Med. 52, 318–328. https://doi.org/10.1038/S12276-020-0405-1.

Leclercq, B., Kluza, J., Antherieu, S., Sotty, J., Alleman, L.Y., Perdrix, E., et al., 2018. Air pollution-derived $PM_{2.5}$ impairs mitochondrial function in healthy and chronic

obstructive pulmonary diseased human bronchial epithelial cells. Environ Pollut 243, 1434–1449. https://doi.org/10.1016/J.ENVPOL.2018.09.062.
Leikauf, G.D., Kim, S.H., Jang, A.S., 2020. Mechanisms of ultrafine particle-induced respiratory health effects. Exp. Mol. Med. 52, 329–337. https://doi.org/10.1038/S12276-020-0394-0.
Li, L.C., Dahiya, R., 2002. MethPrimer:designing primers for methylation PCRs. Bioinformatics 18, 1427–1431. https://doi.org/10.1093/BIOINFORMATICS/18.11.1427.
Li, T., Yu, Y., Sun, Z., Duan, J., 2022. A comprehensive understanding of ambient particulate matter and its components on the adverse health effects based from epidemiological and laboratory evidence. Part. Fibre Toxicol. 19 https://doi.org/10.1186/S12989-022-00507-5.
Long, H., Yin, H., Wang, L., Gershwin, M.E., Lu, Q., 2016. The critical role of epigenetics in systemic lupus erythematosus and autoimmunity. J. Autoimmun. 74, 118–138. https://doi.org/10.1016/J.JAUT.2016.06.020.
McGovern, T., Risse, P.A., Tsuchiya, K., Hassan, M., Frigola, G., Martin, J.G., 2010. LTD4 induces HB-EGF-dependent CXCL8 release through EGFR activation in human bronchial epithelial cells. Am. J. Physiol. Lung Cell Mol. Physiol. 299, 808–815. https://doi.org/10.1152/AJPLUNG.00438.2009/ASSET/IMAGES/LARGE/ZH50121057710008.JPEG.
Misztal, P.K., Lymperopoulou, D.S., Adams, R.I., Scott, R.A., Lindow, S.E., Bruns, T., et al., 2018. Emission factors of microbial volatile organic compounds from environmental bacteria and fungi. Environ. Sci. Technol. 52, 8272–8282. https://doi.org/10.1021/ACS.EST.8B00806.
Miura, T., Onodera, R., Terashima, J., Ozawa, S., Habano, W., 2021. β-naphthoflavone-induced upregulation of CYP1B1 expression is mediated by the preferential binding of aryl hydrocarbon receptor to unmethylated xenobiotic responsive elements. Exp. Ther. Med. 22 https://doi.org/10.3892/ETM.2021.10846.
Morawska, L., Afshari, A., Bae, G.N., Buonanno, G., Chao, C.Y.H., Hänninen, O., et al., 2013. Indoor aerosols: from personal exposure to risk assessment. Indoor Air 23, 462–487. https://doi.org/10.1111/INA.12044.
Nazaroff, W.W., 2023. Ten questions concerning indoor ultrafine particles. Build. Environ. 243, 110641 https://doi.org/10.1016/J.BUILDENV.2023.110641.
Nebert, D.W., 2017. Aryl hydrocarbon receptor (AHR): "pioneer member" of the basic-helix/loop/helix per-Arnt-sim (bHLH/PAS) family of "sensors" of foreign and endogenous signals. Prog. Lipid Res. 67, 38–57. https://doi.org/10.1016/J.PLIPRES.2017.06.001.
Oberdörster, G., Sharp, Z., Atudorei, V., Elder, A., Gelein, R., Kreyling, W., et al., 2004. Translocation of inhaled ultrafine particles to the brain. Inhal. Toxicol. 16, 437–445. https://doi.org/10.1080/08958370490439597.
Paglione, M., Gilardoni, S., Rinaldi, M., Decesari, S., Zanca, N., Sandrini, S., Giulianelli, L., Bacco, D., Ferrari, S., Poluzzi, V., Scotto, F., Trentini, A., Poulain, L., Herrmann, H., Wiedensohler, A., Canonaco, F., Prévôt, A.S.H., Massoli, P., Carbone, C., Facchini, M.C., Fuzzi, S., 2020. The impact of biomass burning and aqueous-phase processing on air quality: a multi-year source apportionment study in the Po Valley, Italy. Atmos. Chem. Phys. 20, 1233–1254. https://doi.org/10.5194/acp-20-1233-2020.
Panni, T., Mehta, A.J., Schwartz, J.D., Baccarelli, A.A., Just, A.C., Wolf, K., et al., 2016. Genome-Wide analysis of DNA methylation and fine particulate matter air pollution in three study populations: KORA F3, KORA F4, and the normative aging study. Environ. Health Perspect. 124, 983–990. https://doi.org/10.1289/EHP.1509966.
Pardo, M., Li, C., He, Q., Levin-Zaidman, S., Tsoory, M., Yu, Q., et al., 2020. Mechanisms of lung toxicity induced by biomass burning aerosols. Part. Fibre Toxicol. 17 https://doi.org/10.1186/S12989-020-0337-X.
Park, M., Joo, H.S., Lee, K., Jang, M., Kim, S.D., Kim, I., et al., 2018. Differential toxicities of fine particulate matters from various sources. Sci. Rep. 8 https://doi.org/10.1038/S41598-018-35398-0.
Pelliccioni, A., Monti, P., Cattani, G., Boccuni, F., Cacciani, M., Canepari, S., et al., 2020. Integrated Evaluation of Indoor Particulate Exposure: The VIEPI Project 12, 9758. https://doi.org/10.3390/su12229758.
Peretz, A., Peck, E.C., Bammler, T.K., Beyer, R.P., Sullivan, J.H., Trenga, C.A., et al., 2007. Diesel exhaust inhalation and assessment of peripheral blood mononuclear cell gene transcription effects: an exploratory study of healthy human volunteers. Inhal. Toxicol. 19, 1107–1119. https://doi.org/10.1080/08958370701665384.
Pinkerton, J.W., Kim, R.Y., Robertson, A.A.B., Hirota, J.A., Wood, L.G., Knight, D.A., et al., 2017. Inflammasomes in the lung. Mol. Immunol. 86, 44–55. https://doi.org/10.1016/J.MOLIMM.2017.01.014.
Reese, S.E., Xu, C.J., den Dekker, H.T., Lee, M.K., Sikdar, S., Ruiz-Arenas, C., et al., 2019. Epigenome-wide meta-analysis of DNA methylation and childhood asthma. J. Allergy Clin. Immunol. 143, 2062–2074. https://doi.org/10.1016/J.JACI.2018.11.043.
Rothhammer, V., Quintana, F.J., 2019. The aryl hydrocarbon receptor: an environmental sensor integrating immune responses in health and disease. Nat. Rev. Immunol. 19, 184–197. https://doi.org/10.1038/S41577-019-0125-8.
Saleh, R., Robinson, E.S., Tkacik, D.S., Ahern, A.T., Liu, S., Aiken, A.C., et al., 2014. Brownness of organics in aerosols from biomass burning linked to their black carbon content. https://doi.org/10.1038/NGEO2220.
Stafoggia, M., Bellander, T., Bucci, S., Davoli, M., de Hoogh, K., de' Donato, F., et al., 2019. Estimation of daily PM10 and PM2.5 concentrations in Italy, 2013-2015, using a spatiotemporal land-use random-forest model. Environ. Int. 124, 170–179. https://doi.org/10.1016/J.ENVINT.2019.01.016.
Stewart, T., 2012. Editorial. Behav. Inf. Technol. 31, 943–945. https://doi.org/10.1080/0144929X.2012.728385.
Targino, A.C., Krecl, P., Oukawa, G.Y., Mollinedo, E.M., 2024. A short climatology of black and brown carbon and their sources at a suburban site impacted by smoke in Brazil. Journal of Environmental Sciences 136, 498–511.
Vogel, C.F.A., Kado, S.Y., Kobayashi, R., Liu, X., Wong, P., Na, K., et al., 2019. Inflammatory marker and aryl hydrocarbon receptor-dependent responses in human macrophages exposed to emissions from biodiesel fuels. Chemosphere 220, 993–1002. https://doi.org/10.1016/J.CHEMOSPHERE.2018.12.178.
Wang, G., Zhang, X., Liu, X., Zheng, J., Chen, R., Kan, H., 2019. Ambient fine particulate matter induce toxicity in lung epithelial-endothelial co-culture models. Toxicol. Lett. 301, 133–145. https://doi.org/10.1016/J.TOXLET.2018.11.010.
Weber, S., Hebestreit, M., Wilms, T., Conroy, L.L., Rodrigo, G., 2013. Comet assay and air–liquid interface exposure system: a new combination to evaluate genotoxic effects of cigarette whole smoke in human lung cell lines. Toxicol Vitr 27, 1987–1991. https://doi.org/10.1016/J.TIV.2013.06.016.
Weichenthal, S., Pinault, L., Christidis, T., Burnett, R.T., Brook, J.R., Chu, Y., et al., 2022. How low can you go? Air pollution affects mortality at very low levels. Sci. Adv. 8, 3381. https://doi.org/10.1126/SCIADV.ABO3381.
Weingartner, E., Saathoff, H., Schnaiter, M., Streit, N., Bitnar, B., Baltensperger, U., 2003. Absorption of light by soot particles: determination of the absorption coefficient by means of aethalometers. J. Aerosol Sci. 34 (10), 1445–1463.
Wells, J.R., Schoemaecker, C., Carslaw, N., Waring, M.S., Ham, J.E., Nelissen, I., et al., 2017. Reactive indoor air chemistry and health-A workshop summary. Int. J. Hyg Environ. Health 220, 1222–1229. https://doi.org/10.1016/J.IJHEH.2017.09.009.
Weng, C.M., Wang, C.H., Lee, M.J., He, J.R., Huang, H.Y., Chao, M.W., et al., 2018. Aryl hydrocarbon receptor activation by diesel exhaust particles mediates epithelium-derived cytokines expression in severe allergic asthma. Allergy 73, 2192–2204. https://doi.org/10.1111/ALL.13462.
Weschler, C.J., Wells, R., 2004. Guest editorial. Indoor Air 14, 373–375. https://doi.org/10.1111/J.1600-0668.2004.00321.X.
WHO global air quality guidelines, 2021. WHO global air quality guidelines: particulate matter (PM2.5 and PM10), ozone, nitrogen dioxide, sulfur dioxide and carbon monoxide. World Health Organization, Geneva. URL https://apps.who.int/iris/handle/10665/345329 (accessed 01.08.22).
Wiedensohler, A., Birmili, W., Nowak, A., Sonntag, A., Weinhold, K., Merkel, M., Wehner, B., Tuch, T., Pfeifer, S., Fiebig, M., Fjæraa, A.M., 2012. Mobility particle size spectrometers: harmonization of technical standards and data structure to facilitate high quality long-term observations of atmospheric particle number size distributions. Atmos. Meas. Tech. 5 (3), 657–685.
Wittkopp, S., Staimer, N., Tjoa, T., Stinchcombe, T., Daher, N., Schauer, J.J., et al., 2016. Nrf2-related gene expression and exposure to traffic-related air pollution in elderly subjects with cardiovascular disease: an exploratory panel study. J. Expo. Sci. Environ. Epidemiol. 26, 141–149. https://doi.org/10.1038/JES.2014.84.
Wolkoff, P., Nøjgaard, J.K., Franck, C., Skov, P., 2006. The modern office environment desiccates the eyes? Indoor Air 16, 258–265. https://doi.org/10.1111/J.1600-0668.2006.00429.X.
Yang, L., Hou, X.-Y., Wei, Y., Thai, P., Chai, F., 2017. Biomarkers of the health outcomes associated with ambient particulate matter exposure. Sci. Total Environ. 579, 1446–1459. https://doi.org/10.1016/j.scitotenv.2016.11.146.
Zhang, Q., et al., 2011. Understanding atmospheric organic aerosols via factor analysis of aerosol mass spectrometry: a review. Anal. Bioanal. Chem. 401 (10), 3045–3067.